Journal of
Polymer Materials

Tech Science Press

DOI: 10.32604/jpm.2024.057953

ARTICLE

Graphite/Polyvinyl Alcohol Hydrogels with Fluoride and Iodine Deionization for Solar-Driven Interfacial Evaporation

Ziyang Qiu[1,2] and Hanjun Yang[1,2,*]

[1]Jiangxi Provincial Key Laboratory of Flexible Electronics, Flexible Electronics Innovation Institute, Jiangxi Science and Technology Normal University, Nanchang, 330013, China

[2]School of Chemistry and Chemical Engineering, Jiangxi Science and Technology Normal University, Nanchang, 330013, China

*Corresponding Author: Hanjun Yang. Email: yanghj@jxstnu.edu.cn

Received: 31 August 2024 Accepted: 31 October 2024 Published: 16 December 2024

ABSTRACT

Hydrogels are emerging as promising candidates for solar-driven interfacial evaporation in water purification. Our research introduces a graphite polyvinyl alcohol hydrogel (GPVA) evaporator designed as a photothermal conversion interface, showcasing high performance with an evaporation rate of 2.43 kg m^{-2} h^{-1} and an efficiency of 91.9% under solar irradiance of 1 kW m^{-2}. The layered graphite structure of the GPVA hydrogel enhances its ion and dye adsorption capabilities, effectively removing fluoride, iodine, and other contaminants from water. In cyclic evaporation tests, the GPVA hydrogel evaporator demonstrated remarkable stability and long-term durability, maintaining an evaporation rate of 2.43 ± 0.11 kg m^{-2} h^{-1}. The straightforward preparation of the GPVA hydrogel positions it as a compelling candidate for treating seawater and wastewater containing specific ions, presenting significant potential for water purification applications.

KEYWORDS

Polyvinyl alcohol; graphite; hydrogel; solar interfacial evaporation; deionization

1 Introduction

Freshwater is one of the most crucial resources for humanity, yet the majority of it is locked away in glaciers, ice caps, and groundwater, leaving only 0.26% of the total water volume on Earth accessible for human use [1–3]. Additionally, human activities have contaminated freshwater resources, exacerbating the issue of freshwater scarcity [4]. Decades ago, attention was drawn to seawater desalination and wastewater treatment technologies for freshwater production, followed by significant progress [5]. However, for some specific water pollutants, we still lack a low-cost and efficient treatment method. In certain regions, severe fluoride and iodide pollution has emerged, affecting the lives of local residents and leading to outbreaks of various diseases [6–8]. Traditional photothermal materials, such as metal oxide [9], carbon materials [10], conducting polymers [11], and composite materials [12], have been engaged in complexation with heavy metal cations. They still face the absence of interaction with anions, especially fluoride and iodide anions, which makes it difficult to reach the eco-friendly

discharge standard in purifying some kind of wastewater from industries and medical institutions [6–8].

Solar evaporation systems based on hydrogels typically combine photothermal fillers (such as carbon materials [13], semiconductors [14], polymers [15], plasmonic metals [16], and nanomaterials [17]) with hydrogel substrates [18,19]. Carbon materials (such as carbon nanotubes [20–22], graphene [23,24], and carbon black [12,25]) have garnered significant attention due to their high light absorption in the visible and near-infrared spectra, allowing efficient heat conversion and enhanced evaporation. They also have a unique ability to adsorb certain pollutants, attracting widespread interest from researchers. However, this is also the key to our research and development of interfacial evaporation materials with fluorine ion and iodide ion adsorption functions.

At the same time, the choice of substrate for solar evaporation materials is also crucial. In recent years, hydrogels have seen rapid development, and here we focus on polyvinyl alcohol (PVA). PVA hydrogel possesses a three-dimensional network structure with activated water states, excellent mechanical/electronic properties [26], and multi-scale tunability, making them widely used in diverse fields such as bioelectronics [27,28], biomedical engineering [29], electrochromics [30], strain sensors [31], as well as water purification [32]. In addition, researchers have achieved remarkable results by designing the structure of solar interfacial evaporation materials or modifying photothermal materials to adjust the overall evaporation efficiency [33–35]. Additionally, Li et al. demonstrated the potential of kaolin-based hydrogels for solar-driven evaporation and heavy metal ion removal [36]. This also highlights the strong potential of hydrogel-based solar evaporation systems for ion adsorption. Utilizing solar-driven interfacial evaporation technology to purify this wastewater seems a promising pathway. However, challenges such as high manufacturing costs, complex processes, and environmental impacts still exist, emphasizing the urgent need for more economical, efficient, and environmentally friendly multifunctional solar evaporators to address widespread water pollution and freshwater resource shortages.

This study employs chemical and physical dual-crosslinking methods to prepare a graphite/PVA (GPVA) hydrogel. PVA hydrogel is known for its excellent mechanical and overall performance and is widely used in various studies. In this research, graphite is used as the photothermal material. Through mechanical stirring, a finely porous structure is imparted to the evaporator, combining the characteristics of both fundamental materials to endue GPVA stretchable properties, salt resistance, and the ability to purify fluoride- and iodine-contaminated wastewater. The solar-driven interfacial evaporation system exhibits an evaporation rate of 2.43 kg m^{-2} h^{-1} and an efficiency of 91.9% under 1 kW m^{-2} solar radiation. The evaporator shows high stability, maintaining a stable evaporation rate during a ten-hour consecutive solar evaporation test which collects the data once per hour. The solar evaporator also demonstrates significant potential in solar seawater desalination.

2 Experimental

2.1 Materials

Polyvinyl alcohol (Mw: 146,000–186,000, >99% hydrolyzed), hydrochloric acid (HCl, 37%), and glutaraldehyde (GA, 50% in H_2O) were obtained from Aladdin (Shanghai, China). Graphite, 99.95% (metal basis), 325 mesh natural flake graphite, was produced by Shanghai Titan Technology Co, Ltd., Shanghai, China. All chemicals used in this work were used directly without further purification. All solutions were prepared with distilled water during the whole experiment.

2.2 Preparation Steps of GPVA Hydrogel

First, we prepared a 10 wt% PVA solution by weighing 1.1 g of PVA powder and adding it to 10 mL of deionized water. We then heated the mixture in a water bath at 90°C for 1.5 h while continuously stirring. We added varying amounts of graphite (0.28, 0.43, 0.58, 0.74, 0.90 g) into this PVA solution, then mixed thoroughly to prepare graphite/PVA solutions with different concentrations (2.50, 3.75, 5.00, 6.25, 7.50 wt%). Next, we added 10 μL of glutaraldehyde crosslinking agent and 10 μL of hydrochloric acid catalyst to form mixture solution. We poured the mixture into molds and performed freeze-thaw cycles (freezing for 11 h, thawing for 3 h, and repeating this process 3 times). Finally, we immersed the graphite/PVA hydrogels (GPVA) with different graphite contents in deionized water and stirred for 1 h to remove any residual glutaraldehyde crosslinking agent and hydrochloric acid catalyst, resulting in the final GPVA hydrogel product.

2.3 Characterization

The morphology and structure of the hydrogel were examined by us using field emission scanning electron microscopy (Nova Nano-SEM 230, FEI, Hillsboro, NH, USA). We measured the reflectance and transmittance spectra of the samples using a UV-Vis-NIR spectrophotometer (Cary 7000, Agilent, Santa Clara, CA, USA) combined with an integrating sphere (250–2500 nm). Absorbance (A) was calculated by us using Eq. (1):

$$A = 1 - T - R \tag{1}$$

where R and T represent the reflectance and transmittance of the hydrogel, respectively. We monitored the temperature distribution of the samples in use using a thermal imaging scanner. We measured the ion concentrations of F^-, I^-, Na^+, and K^+ in the simulated wastewater after treatment with GPVA using ion chromatography (ICS-5000+, Thermo Fisher Scientific, Waltham, MA, USA). The concentrations of RhB and MB before and after purification were determined by us using a UV-visible absorption spectrophotometer (TU-1900, Puxi, Beijing, China).

2.4 Solar Evaporation Test Experiment

All simulated solar evaporation experiments were conducted in a laboratory environment (room temperature 25°C, humidity 40%). We used a solar simulator (CEL-HXUV300-T3, Education Light Co., Beijing, China) with an output simulated solar flux of 1 kW m^{-2} and an AM 1.5 G filter. The solar flux was measured by us using an automatic optical power meter (CEL-NP2000-2A, Education Light Co., Beijing, China). A foam board with a diameter of approximately 4 cm and a thickness of about 3 mm was used as a support. We cut out a 2 cm × 2 cm square cavity from the foam board to embed the prepared GPVA. The foam board with the embedded GPVA was then placed by us on the surface of a container filled with water. The assembled sample was placed on an electronic balance (Sartorius BAS223, accuracy: 1 mg), and we used an infrared thermal imaging camera (HM-TPK20-3AQF/W, HIKMICRO, Hangzhou, China) to record the surface temperature and continuously monitor the loss of water weight.

3 Results and Discussion

3.1 Preparation of GPVA Hydrogel

The preparation process of the GPVA hydrogel is illustrated in Fig. 1a. Graphite powder is added to the prepared PVA solution and then mixes rapidly using a stirring machine, creating a solution filled with small bubbles and increasing the water capacity of the GPVA hydrogel. Next, the crosslinking agent glutaraldehyde and the catalyst hydrochloric acid are added. After we thoroughly mix, the GPVA solution is poured into prepared molds and freezes at −20°C for 11 h, then thaws for 3 h.

This process repeats three times, allowing the GPVA hydrogel to form both chemical and physical crosslinks, resulting in a robust mechanical structure (Fig. 1b). Finally, the prepared GPVA is immerses in deionized water and we stir it for 1 h to remove any residual glutaraldehyde and hydrochloric acid, resulting in the final GPVA hydrogel product.

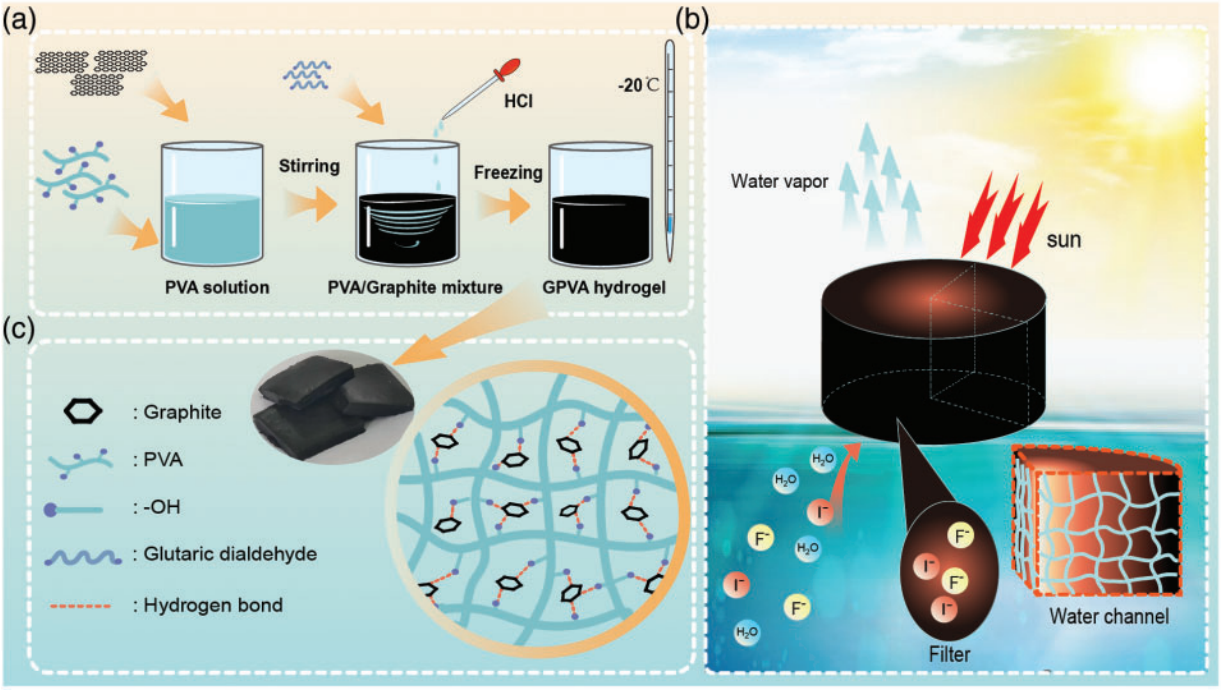

Figure 1: Preparation and practical application schematic of GPVA. (a) Preparation process of GPVA. (b) Schematic of the microscopic network of GPVA and a photograph of the actual material. (c) Schematic diagram of GPVA practical application under sunlight

Graphite provides excellent photothermal effects. It also offers adsorption and filtration capabilities to the GPVA hydrogel. Graphite consists of multiple parallel layers of carbon atoms, which interact through van der Waals forces. Each layer of carbon atoms is arranged in a hexagonal lattice, forming a strong π-bonding system. This strong π bonding system is conducive to the adsorption of substances [37]. Additionally, the spaces between the layers of graphite offer enough surface area for molecule adsorbing. The carbon atoms in the graphite layer are rich in π electrons, allowing them to bond with organic molecules through π-π interactions, which gives graphite a certain adsorption capacity [38]. This characteristic is evident in practical applications.

During practical solar evaporation applications, the fine porous structure in GPVA not only provides a rough surface that enhances solar absorption but also offers ample channels for steam escape (Figs. 1c and 2a).

3.2 Characterization of GPVA Hydrogels

Observations of GPVA (Fig. 2a) reveal many pores on its surface. SEM (Scanning Electron Microscopy) imaging at a resolution of 20 nm reveals a densely porous surface structure of GPVA (Fig. 2b). This is mainly due to the vigorous mechanical stirring during the mixing of PVA with graphite, which creates a three-dimensional interconnected porous structure within the hydrogel. In order to verify whether graphite and PVA are mixed uniformly, we conduct a mapping test on GPVA.

When observing the distribution of C and O in GPVA (Fig. 2c,d), we find that these two elements show a uniform distribution in GPVA, indicating the successful preparation of GPVA.

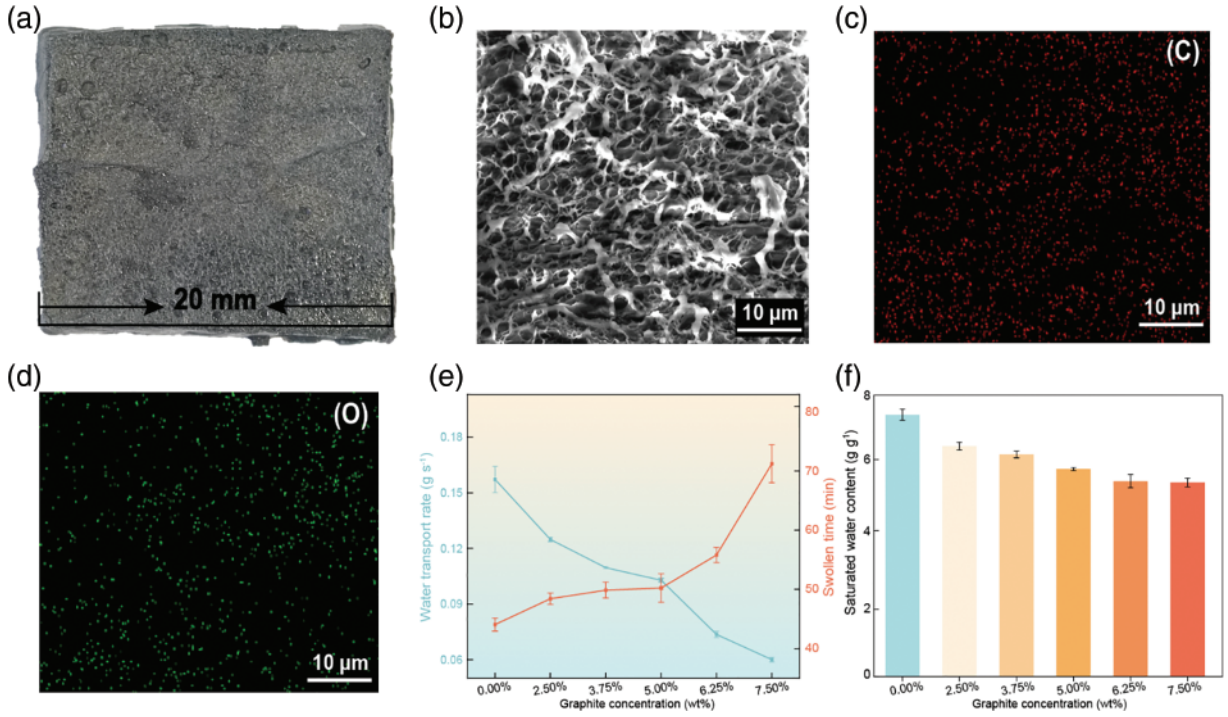

Figure 2: Photographs, SEM, and water transport capabilities of the samples. (a) Photograph of the GPVA sample. (b) SEM image of GPVA. (c, d) Element mapping for GPVA (C and O). (e) Time to reach saturation and water transport rate of dry gels with different graphite contents. (f) Relationship between the saturated water content of GPVA hydrogel and graphite content (The 0.00% graphite GPVA in the figure is PVA.)

3.3 Solar Steam Generation Performance of GPVA Hydrogel Evaporators

In order to explore the influence of graphite content on the evaporation performance of GPVA, we first study the water transport properties of GPVA with different graphite contents.

We evaluate the effect of graphite content on the saturated water content (Q_s) of the resulting GPVA hydrogel after further swelling in water. As shown in Fig. 2e, when the graphite content in GPVA increases to 7.50%, the time for GPVA to swell to saturation also shows a leap-forward increase. And it can be seen from Fig. 2f that the increase in graphite content also leads to a decrease in the water content of GPVA. The saturated water content (Q_s) can be calculated using the Eq. (2):

$$Q_s = \frac{(m_1 - m_2)}{m_2} \tag{2}$$

where m_1 is the mass of the fully swollen GPVA, and m_2 is the dry weight of GPVA.

GPVA exhibits maximum equilibrium water content of 6.09 g g^{-1}, reaching near-saturation within 44 min. Concurrently, the saturation kinetics from dry to saturated states were monitored, showing a water absorption rate of up to 0.15 g s^{-1}.

We test the photothermal absorption conversion performance of GPVA. As shown in Fig. 3a, the overall light absorption efficiency of PVA reaches 99.9% after the addition of photothermal graphite.

In addition, we prepared GPVA hydrogels with different graphite contents and used them to calculate the evaporation rate under the condition of being tested for one hour under one sun. It is found through comparison that the GPVA with a graphite content of 6.25% has the best evaporation rate (Fig. 3b), which could reach 2.43 kg m^{-2} h^{-1}. Fig. 3c shows real-time thermal imaging of GPVA, where the temperature rises from 26.5°C to 42.6°C within an hour, visually demonstrating GPVA is photothermal conversion ability, which is crucial for interface solar evaporation materials.

We systematically test the evaporation performance of GPVA. Firstly, under different solar flux light intensities, the evaporation performance increases proportionally, reflected in the amount of water evaporation (Fig. 3d) and temperature rise. Under 1.5 suns, the temperature can reach 45.1°C (Fig. 3e), and the evaporation rate can reach 3.17 kg m^{-2} h^{-1} (Fig. 3f). The evaporation rate (m) is calculated by the Eq. (3):

$$m = \frac{\Delta m}{\mathrm{A}t} \tag{3}$$

In the formula, Δm represents the change in the mass of water, A represents the evaporation area of the hydrogel, and t represents the time of evaporation.

Comparing the natural evaporation in the dark environment of GPVA hydrogels with 2.50%, 3.75%, 5.00%, 6.25%, 7.50% graphite content, we find that PVA with 6.25% graphite has the highest dark evaporation amount (Fig. 3g). By comparing dark evaporation enthalpy, we discover that GPVA with 6.25% graphite content requires the least energy for evaporation (Fig. 3h). Dark evaporation enthalpy can be calculated using the Eq. (4):

$$\Delta H_{equ} = \frac{m_0}{m_g} \times \Delta H_{vap} \tag{4}$$

In the formula, ΔH_{vap} and m_0 represent the enthalpy of evaporation of bulk water and the mass change, respectively, while m_g denotes the mass change of the hydrogel.

Comparing the evaporation efficiency of GPVA hydrogels with 2.50%, 3.75%, 5.00%, 6.25%, and 7.50% graphite content (Fig. 3i), we can conclude that GPVA with 6.25% graphite content has the highest efficiency, reaching 91.9%. The evaporation efficiency (η) can be calculated using the Eq. (5):

$$\eta = \frac{m\Delta H_{equ}}{C_{opt}P_0} \tag{5}$$

where m is the evaporation rate of GPVA, P_0 is the solar irradiance power (1 kW m^{-2}), and C_{opt} is the optical concentration.

3.4 Adaptability of GPVA Hydrogel Evaporators

The development of interface solar evaporation materials cannot be separated from practical application capability testing. Here, we test the GPVA using the evaporation schematic in Fig. 4a. Sunlight passing through a colorless glass plate allows the GPVA hydrogel to receive sunlight, while water vapor condenses into droplets on the glass, which is then collected by the collection device for purified water.

In practical applications, the material is required to withstand external forces without being easily damaged. We carry out a simple bending, pulling, twisting and rolling test on GPVA hydrogel (Fig. 4b) and find that no irreversible damage was caused to it. Moreover, we use GPVA as the linking material to conduct a pull-up test with a 1 kg weight. Fig. 4c shows that GPVA withstands the tension, and GPVA is also stretched from 0.5 to 1.5 cm, indicating that it is able to mechanical deform and can withstand normal operation during actual use.

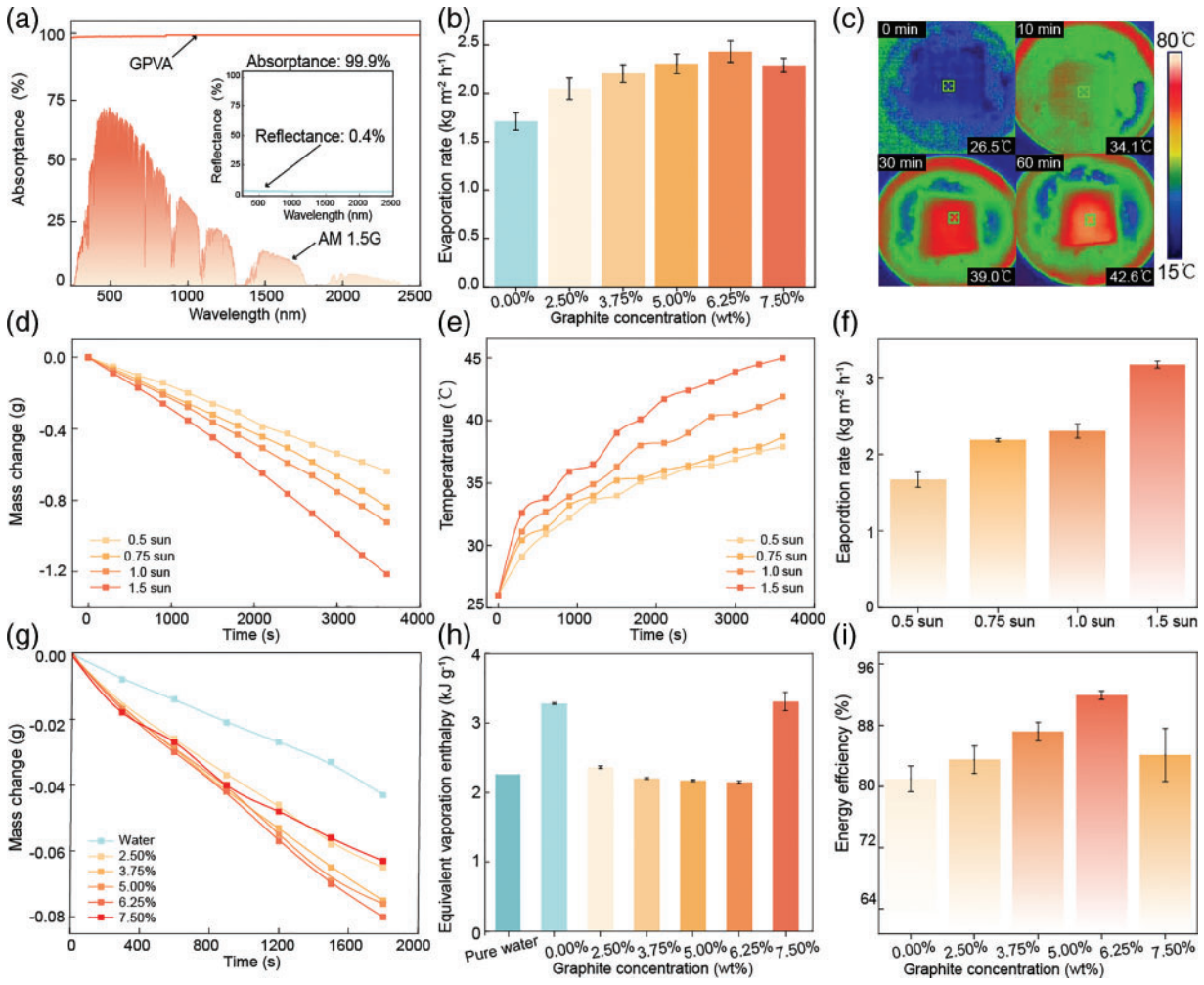

Figure 3: Solar steam generation performance of varying GPVA hydrogel. (a) UV-vis-NIR absorptance and reflectance (Inset) spectra of GPVA hydrogel sheets with a thickness of 5 mm in the wavelength range of 250∼2500 nm. (b) The evaporation rates of PVA and GPVA with different graphite contents (2.50%, 3.75%, 5.00%, 6.25%, 7.50%) under the solar irradiation power of 1.0 kW m^{-2}. (c) Temperature records of GPVA with 6.25% graphite content under solar irradiation for 0, 10, 30, and 60 min. (d) Water mass change of GPVA hydrogel under different solar irradiance powers (0.75–1.5 suns, 0.75–1.5 kW m^{-2}) over 1 h. (e) Temperature changes of GPVA hydrogel under different solar irradiance powers (0.75–1.5 suns, 0.75–1.5 kW m^{-2}) over 1 h. (f) Evaporation rates were calculated from GPVA hydrogel under different solar irradiance powers (0.75–1.5 suns, 0.75–1.5 kW m^{-2}) over 1 h. (g) Mass changes of GPVA with different graphite contents (2.50%, 3.75%, 5.00%, 6.25%, 7.50%) under dark evaporation for 0.5 h. (h) Dark evaporation enthalpy was calculated for pure water, PVA, and GPVA with different graphite contents. (i) Energy efficiency calculated for GPVA with different graphite contents (2.50%, 3.75%, 5.00%, 6.25%, 7.50%)

Solar interface evaporation materials are often used in seawater environments, so adaptability to seawater is essential. We test the evaporation rates of GPVA hydrogel in different concentrations of 3.5, 5, and 10 wt% seawater (Fig. 4d). We also test the seawater salt resistance by sprinkling sea salt on the GPVA surface and conducting solar simulation evaporation tests. The sea salt gradually dissolves into the GPVA surface within 70 min and disappears (Fig. 4e), indicating that the high-concentration

seawater solution can pass through the water transport channels of the GPVA hydrogel. Although seawater concentration has some effect on GPVA hydrogel, the overall impact is minimal, proving the salt resistance of GPVA hydrogel. These tests demonstrate the practical application capability of GPVA hydrogel.

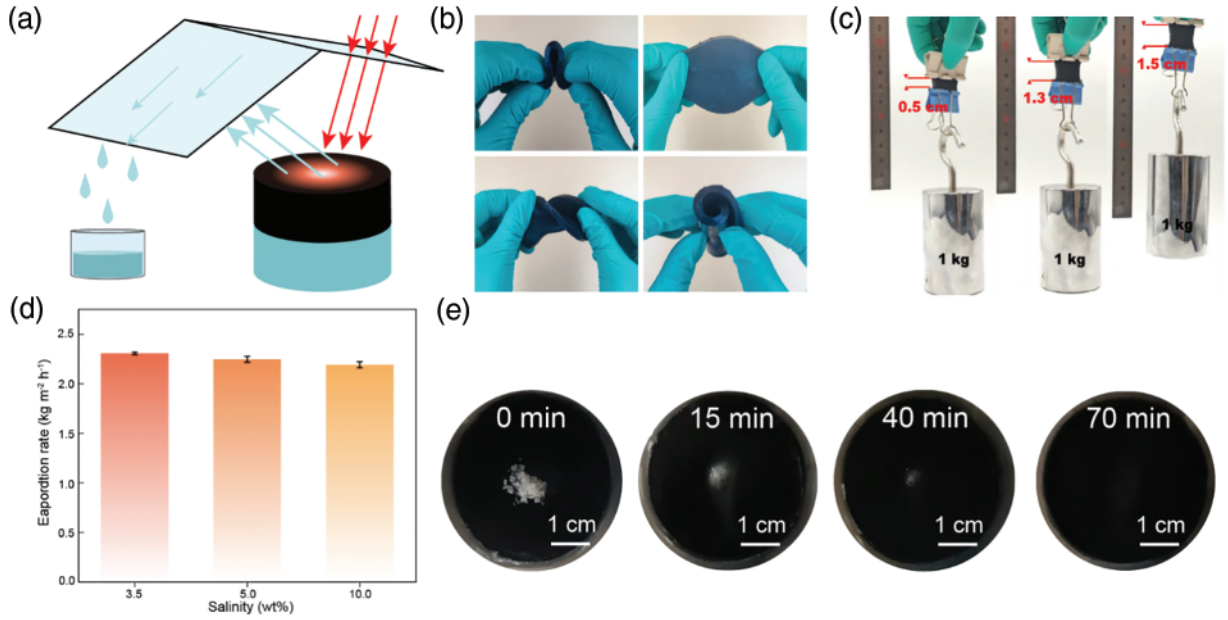

Figure 4: Mechanical deformation and salt resistance of GPVA hydrogel. (a) Schematic diagram of the solar evaporation device. (b) Photos of GPVA hydrogel in bending, stretching, twisting, rolling and recovered image. (c) GPVA is used as a linking material to lift a 1 kg weight, stretching it from 0.5 to 1.5 cm. (d) Evaporation rates of seawater with different salinities. (e) Photos of salt dissolution on the surface of GPVA hydrogel at 0, 15, 40, and 70 min

3.5 GPVA Hydrogel Evaporator Water Purification Capacity

Long-term stable evaporation performance is a key indicator for assessing the water purification capability of interface solar evaporation materials. We conduct ten tests of wastewater evaporation with GPVA. The evaporation rate remained at 2.43 ± 0.11 kg m^{-2} h^{-1} (Fig. 5a), demonstrating that the GPVA hydrogel has stable evaporation capabilities, which is fundamental for its water purification ability.

To demonstrate the efficacy of GPVA in removing organic pollutants, we add representative dyes such as rhodamine (RB) and methylene blue (MB) with a concentration of 20 mg L^{-1} to wastewater samples. Visual inspection (Fig. 5b,c) shows that the GPVA hydrogel solar steam generator effectively removes all the dyes. Further UV-visible spectroscopy of the purified wastewater confirms the complete removal of these organic pollutants (Fig. 5b,c).

When testing the water purification capability of GPVA (Fig. 5d), we first measure the resistance of 3.5 wt% seawater using a multimeter, which was 74.4 kΩ. After purification, the resistance of the 3.5 wt% seawater increases to 585.0 kΩ. This significant increase in resistance indicates a substantial reduction in ion content in the purified water. Finally, the purified seawater is compared with tap water (resistance of 198.2 kΩ) and deionized water (resistance of 1576.0 kΩ), showing that the ion content in the purified seawater was lower than that of tap water. These results confirm the practical application potential of GPVA hydrogel for seawater purification.

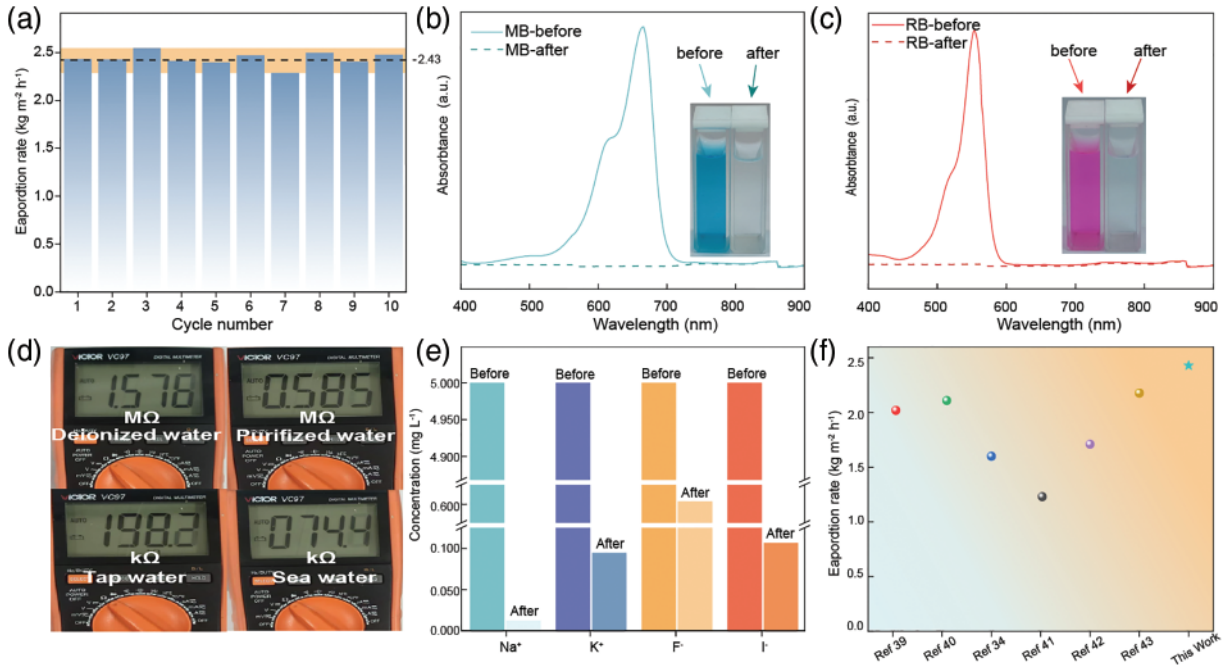

Figure 5: Testing the water purification performance of GPVA hydrogel. (a) Data from ten one-hour evaporation tests of GPVA hydrogel, with the evaporation rate stabilizing around 2.43 kg m^{-2} h^{-1}. (b) UV-visible absorbance and digital images of wastewater samples containing methylene blue (20 mg L^{-1}) before and after solar purification. (c) UV-visible absorbance and digital images of wastewater samples containing rhodamine (20 mg L^{-1}) before and after solar purification. (d) Photos of the resistivity of purified seawater compared to deionized water, tap water, and seawater. (e) Na^+, K^+, F^-, I^- concentration of sewage before and after purification. (f) Steam generation performance of GPVA compared with previous reports under 1 kW m^{-2} simulated solar irradiation

Additionally, we test the special water purification capability of GPVA by purifying industrial wastewater containing F^-, I^-, Na^+, and K^+. We measure the concentrations of these ions in purified water using ion chromatography (IC) and compared the concentrations before and after purification. The results indicate a significant reduction in the levels of these ions in the purified water, with Na^+ concentration decreasing from 5 to 0.001 mg L^{-1}, K^+ concentration dropping from 5 to 0.007 mg L^{-1}, F^- concentration reducing from 5 to 0.612 mg L^{-1}, and I^- concentration decreasing from 5 to 0.008 mg L^{-1} (Fig. 5e). By comparing the concentration changes of these ions, we further demonstrate the potential of GPVA to purify specific wastewater. This makes it promising for practical applications.

Finally, the evaporation rate of GPVA is shown in Fig. 5f. It can be seen that the evaporation rate of GPVA reaches as high as 2.43 kg m^{-2} h^{-1}. To demonstrate the superiority of GPVA-based solar interfacial evaporation, we compare its evaporation rate with those reported in previous studies (Fig. 5f). The results show that GPVA exhibits a higher evaporation rate compared to other recently reported hydrogel-based solar vaporizers, including graphene [34,39,40], PEDOT:PSS [41], carbon nanotubes [42], and copper sulfide [43]. Therefore, GPVA has certain advantages as a solar interfacial evaporation material, and its ability to purify fluoride and iodine ions further highlights the innovation of GPVA.

4 Conclusions

In summary, we have successfully developed GPVA hydrogel, a pioneering solar evaporation material, which is crafted through the meticulous blending of PVA solution and graphite powder. These two materials yield a robust structure that is both chemically and physically cross-linked. This unique composite structure, enriched with graphite powder, significantly amplifies the photothermal conversion efficiency of GPVA while also imparting exceptional purification capacity. Consequently, the GPVA hydrogel demonstrates evaporation performance scales up with the augmentation of graphite content and solar radiation intensity, peaking at an impressive 91.9% evaporation efficiency. Furthermore, GPVA hydrogels can withstand bending, pulling, twisting, rolling, and the tension from a 1 kg weight illustrates its sturdy and robust characteristics. In addition to its strong potential in seawater desalination, its excellent salt tolerance also makes it suitable for operation in harsh environments. In practical scenarios, GPVA hydrogel shines as a reliable wastewater evaporator, proficiently eliminating ions and organic pollutants, thereby demonstrating unparalleled water purification prowess. This study provides a simple, low-cost preparation process to form solar-driven evaporators with high performance and long-term stability, which develops a promising strategy for practice application.

Acknowledgement: We heartfelt gratitude Prof. Baoyang Lu (Jiangxi Science and Technology Normal University) for valuable discussions; extends their thank to Zheng Li, Xinye Xu, Junxiao Qiu, Qisheng Ma and Boyu Zhang for the invaluable assistance rendered throughout the course of this research.

Funding Statement: This work was financially supported by the Jiangxi Provincial Key Laboratory of Flexible Electronics (20212BCD42004 & 20242BCC32010), the Doctoral Start-Up Funding of Jiangxi Science & Technology Normal University (2022BSQD10), and the Open Fund of Jiangxi Key Laboratory of Flexible Electronics (2023KFJJ15).

Author Contributions: Ziyang Qiu: Conceptualization, Methodology, Investigation, Validation, Formal Analysis, Investigation, Writing—Original Draft. Hanjun Yang: Formal Analysis, Methodology, Validation, Supervision. All authors reviewed the results and approved the final version of the manuscript.

Availability of Data and Materials: All data generated or analyzed during this study are included in this published article.

Ethics Approval: Not applicable.

Conflicts of Interest: The authors declare no conflicts of interest to report regarding the present study.

References

1. Mekonnen MM, Hoekstra AY. Sustainability: four billion people facing severe water scarcity. Sci Adv. 2016;2(2):1500323. doi:10.1126/sciadv.1500323.
2. Scanlon BR, Fakhreddine S, Rateb A, Graaf ID, Famiglietti J, Gleeson T, et al. Global water resources and role of groundwater in a more resilient water future. Nat Rev Earth Env. 2023;4(2):87–101. doi:10.1038/s43017-022-00378-6.
3. Cunillera-Montcusí D, Beklioğlu M, Cañedo-Argüelles M, Jeppesen E, Ptacnik R, Amorim CA, et al. Freshwater salinisation: a research agenda for a saltier world. Trends Ecol Evol. 2022;37(5):440–53. doi:10.1016/j.tree.2021.12.005.
4. Rodell M, Famiglietti JS, Wiese DN, Reager JT, Beaudoing HK, Landerer FW, et al. Emerging trends in global freshwater availability. Nature. 2018;557(7707):651–9. doi:10.1038/s41586-018-0123-1.

5. Gleick PH. Transitions to freshwater sustainability. Proc Natl Acad Sci U S A. 2018;115(36):8863–71. doi:10.1073/pnas.1808893115.
6. Yu Y, Cui S, Fan R, Fu Y, Liao Y, Yang J. Distribution and superposed health risk assessment of fluorine co-effect in phosphorous chemical industrial and agricultural sources. Environ Pollut. 2020;262:114249. doi:10.1016/j.envpol.2020.114249.
7. Chakraborty A. Excess iodine exposure: an emerging area of concern for male reproductive physiology in the post-salt iodization era. Asian Pac J Reprod. 2021;10(3):10. doi:10.4103/2305-0500.316622.
8. Rajak P, Roy S, Khatun S, Mandi M, Ganguly A, Das K, et al. Fluoride contamination, toxicity and its potential therapeutic agents. Toxic Int. 2023;29(4):553–65. doi:10.18311/ti/2022/v29i4/30844.
9. Xu X, Zhao Q, Liu Q, Qiu J, Li J, Zheng W, et al. Full-spectrum-responsive Ti_4O_7-PVA nanocomposite hydrogel with ultrahigh evaporation rate for efficient solar steam generation. Desalination. 2024;577:117400. doi:10.1016/j.desal.2024.117400.
10. Hu Y, Yao H, Liao Q, Lin T, Cheng H, Qu L. The promising solar-powered water purification based on graphene functional architectures. EcoMat. 2022;4:12205. doi:10.1002/eom2.12205.
11. Li C, Goswami Y, Stefanakos E. Solar assisted sea water desalination: a review. Renew Sust Energ Rev. 2013;19:136–63. doi:10.1016/j.rser.2012.04.059.
12. Guo Y, Li C, Wei P, Hou K, Zhu M. Scalable carbon black deposited fabric/hydrogel composites for affordable solar-driven water purification. J Mater Sci Technol. 2022;106:10–8. doi:10.1016/j.jmst.2021.07.032.
13. Guan W, Guo Y, Yu G. Carbon materials for solar water evaporation and desalination. Small. 2021;17:2007176. doi:10.1002/smll.202007176.
14. He D, Yang H, Jin D, Qu J, Yuan X, Zhang Y, et al. Rapid water purification using modified graphitic carbon nitride and visible light. Appl Catal B. 2021;285:119864. doi:10.1016/j.apcatb.2020.119864.
15. Zhao Q, Wu Z, Xu X, Yang R, Ma H, Xu Q, et al. Design of poly (3,4-ethylenedioxythiophene): polystyrene sulfonate-polyacrylamide dual network hydrogel for long-term stable, highly efficient solar steam generation. Sep Purif Technol. 2022;300:121889. doi:10.1016/j.seppur.2022.121889.
16. Bae K, Kang G, Cho SK, Park W, Kim K, Padilla WJ. Flexible thin-film black gold membranes with ultrabroadband plasmonic nanofocusing for efficient solar vapour generation. Nat Commun. 2015;6:10103. doi:10.1038/ncomms10103.
17. Cui X, Ruan Q, Zhuo X, Xia X, Hu J, Fu R, et al. Photothermal nanomaterials: a powerful light-to-heat converter. Chem Rev. 2023;123(11):6891–952. doi:10.1021/acs.chemrev.3c00159.
18. Zhao F, Guo Y, Zhou X, Shi W, Yu G. Materials for solar-powered water evaporation. Nat Rev Mater. 2020;5(5):388–401. doi:10.1038/s41578-020-0182-4.
19. Tao P, Ni G, Song C, Shang W, Wu J, Zhu J, et al. Solar-driven interfacial evaporation. Nat Energy. 2018;3(12):1031–41. doi:10.1038/s41560-018-0260-7.
20. Zhou S, Zhang J, Wang C, Wu C, Zhang X, Yang Z, et al. Extremely black carbon nanotube materials with three-dimensional networks for highly efficient solar-driven vapor generation. Nanoscale. 2022;14(46):17438–46. doi:10.1039/d2nr04857d.
21. Nam S, Park C, Sunwoo SH, Kim M, Lee H, Lee M, et al. Soft conductive nanocomposites for recording biosignals on skin. Soft Sci. 2023;3:28. doi:10.20517/ss.2023.19.
22. Luo W, Xuan X, Shen J, Cheng P, Wang D, Schaaf P, et al. High performance photothermal carbon nanotubes/nanostructured hydrogel for solar electricity production and solar water sterilization. Appl Surf Sci. 2024;643:158680. doi:10.1016/j.apsusc.2023.158680.
23. Yu H, Gai M, Liu L, Chen F, Bian J, Huang Y. Laser-induced direct graphene patterning: from formation mechanism to flexible applications. Soft Sci. 2023;3:4. doi:10.20517/ss.2022.26.
24. Yang J, Chen D, Zhu Y, Zhang Y, Zhu Y. 3D-3D porous Bi_2WO_6/graphene hydrogel composite with excellent synergistic effect of adsorption-enrichment and photocatalytic degradation. Appl Catal B-Environ. 2017;205:228–37. doi:10.1016/j.apcatb.2016.12.035.
25. Ying L, Huang Z, Dong Y, Lin F, Ding J, Wang W, et al. Hybrid nanoarchitectonics of carbon/titanium carbide integrated hydrogel/melamine foam for highly efficient solar steam and thermoelectric power generation. Desalination. 2023;549:116328. doi:10.1016/j.desal.2022.116328.
26. Yang Y, Xiong Z, Wang Z, Liu Y, He Z, Cao A, et al. Super-adsorptive and photo-regenerable carbon nanotube based membrane for highly efficient water purification. J Memb Sci. 2021;621:119000. doi:10.1016/j.memsci.2020.119000.

27. Ke X, Mu X, Chen S, Zhang Z, Zhou J, Chen Y, et al. Reduced graphene oxide reinforced PDA-Gly-PVA composite hydrogel as strain sensors for monitoring human motion. Soft Sci. 2023;3(3):21. doi:10.20517/ss.2023.14.
28. Yu J, Wan R, Tian F, Cao J, Wang W, Liu Q, et al. 3D printing of robust high-performance conducting polymer hydrogel-based electrical bioadhesive interface for soft bioelectronics. Small. 2024;20(19):2308778. doi:10.1002/smll.202308778.
29. Ma H, Hou J, Xiao X, Wan R, Ge G, Zheng W, et al. Self-healing electrical bioadhesive interface for electrophysiology recording. J Colloid Interf Sci. 2024;654:639–48. doi:10.1016/j.jcis.2023.09.190.
30. Zheng W, Wang L, Jiao H, Wu Z, Zhao Q, Lin T, et al. A cost-effective, fast cooling, and efficient anti-inflammatory multilayered topological hydrogel patch for burn wound first aid. Chem Eng J. 2023;455:140553. doi:10.1016/j.cej.2022.140553.
31. Luo X, Wan R, Zhang Z, Song M, Yan L, Xu J, et al. 3D-printed hydrogel-based flexible electrochromic device for wearable displays. Adv Sci. 2024;11:2404679. doi:10.1002/advs.202404679.
32. Zhang Z, Chen G, Xue Y, Duan Q, Liang X, Lin T, et al. Fatigue-resistant conducting polymer hydrogels as strain sensor for underwater robotics. Adv Funct Mater. 2023;33:2305705. doi:10.1002/adfm.202305705.
33. Zhao Q, Liu J, Wu Z, Xu X, Ma H, Hou J, et al. Robust PEDOT: pSS-based hydrogel for highly efficient interfacial solar water purification. Chem Eng J. 2022;442:136284. doi:10.1016/j.cej.2022.136284.
34. Wang Y, Wu X, Wu P, Yu H, Zhao J, Yang X, et al. Salt isolation from waste brine enabled by interfacial solar evaporation with zero liquid discharge. J Mater Chem A. 2022;10:14470–8. doi:10.1039/D2TA03004G.
35. Qiu J, Xu X, Li Z, Hu Y, Liu G, Lv X, et al. A solar-electric dual-driven microporous hydrogel evaporator for all-weather highly efficient water purification. Nano Energy. 2024;130:110057. doi:10.1016/j.nanoen.2024.110057.
36. Li Z, Qiu J, Xu X, Wan R, Yao M, Wang H, et al. Solar driven kaolin-based hydrogels for efficient interfacial evaporation and heavy metal ion adsorption from wastewater. Sep Purif Technol. 2025;354:129243. doi:10.1016/j.seppur.2024.129243.
37. Jara AD, Betemariam A, Woldetinsae G, Kim J. Purification, application and current market trend of natural graphite: a review. Int J Min Sci Technol. 2019;29:671–89. doi:10.1016/j.ijmst.2019.04.003.
38. Doondani P, Jugade R, Gomase V, Shekhawat A, Bambal A, Pandey S. Chitosan/Graphite/Polyvinyl alcohol magnetic hydrogel microspheres for decontamination of reactive orange 16 dye. Water-Sui. 2022;14:3411. doi:10.3390/w14213411.
39. Liu C, Cai C, Ma F, Zhao X, Ahmad H. Accelerated solar steam generation for efficient ions removal. J Colloid Interf Sci. 2020;560:103–10. doi:10.1016/j.jcis.2019.10.055.
40. Gong L, Sun J, Zheng P, Lin F, Yang G, Liu Y. Two birds one stone: facile and controllable synthesis of the Ag quantum dots/reduced graphene oxide composite with significantly improved solar evaporation efficiency and bactericidal performance. ACS Appl Mater Interfaces. 2021;13:17649–57. doi:10.1021/acsami.1c02480.
41. Zhao X, Liu C. Overcoming salt crystallization with ionic hydrogel for accelerating solar evaporation. Desalination. 2020;482:114385. doi:10.1016/j.desal.2020.114385.
42. An N, Jiang Y, Wang Z, Sun Q, Guo B, Gao B, et al. Efficient water purification and desalination using hydrogel and aerogel solar evaporators based on different carbon materials. Sep Purif Technol. 2022;301:122003. doi:10.1016/j.seppur.2022.122003.
43. Wang Z, Zhang X, Lian S, Yao J. Copper sulfide integrated functional cellulose hydrogel for efficient solar water purification. Carbohyd Polym. 2023;319(6):121161. doi:10.1016/j.carbpol.2023.121161.